Turbulence, Heat and Mass Transfer 6
K. Hanjalić, Y. Nagano and S. Jakirlić (Editors)

Dynamics of Large-Scale Structures and Heat Transfer in Turbulent Mixed Convection

A. Westhoff[1], D. Schmeling[1], J. Bosbach[1] and C. Wagner[1]

[1]*German Aerospace Center (DLR), Institute of Aerodynamics and Flow Technology, Bunsenstr. 10, D-37073 Göttingen, Germany, andreas.westhoff@dlr.de*

Abstract — Low frequency oscillations in the heat transfer of mixed convection in a rectangular cavity with an aspect ratio of $\Gamma_{xz} = 1$ and $\Gamma_{yz} = 5$ have been observed. Mixed convective flow at $Ra = 2.4 \times 10^8$, $Re = 1.0 \times 10^4$, $Ar = 3.3$ and $Pr \approx 0.7$ was studied to determine the nature of these oscillations. Therefore Particle Image Velocimetry (PIV) and temperature measurements have been performed under ambient and heigh pressure conditions. The PIV results have been analysed using Proper Orthogonal Decomposion (POD) to identify the characteristic frequencies of the coherent large-scale structures dynamics and compared their dynamics with the low frequency oscillations found in the heat transfer.

1. Introduction

Convection is the prevalent transport mechanism of heat in many flows. Often this type of heat transfer depends on the dynamics of large-scale flow structures. In mixed convection (MC) the heat transfer is determined by the interaction of forced convection (FC) and thermal convection (TC). Turbulent MC has attracted a lot of interest during the last decades and is of utmost importance e.g. in geophysics, astrophysics, indoor climatisation or in industrial processes and applications [1].

In this study we investigate the influence of the dynamics of the Large Scale Circulations (LSC), also known as "mean wind" on the heat transfer. Therefore a simple geometrical arrangement was chosen to investigate heat transfer and structure formation in MC: a fluid layer confined between two isothermal horizonal plates heated from below and cooled from above is exposed to FC in a rectangular enclosure.

This system is defined by five dimensionless parameters, i.e. the Rayleigh number $Ra \equiv \Delta T \beta g H^3 / \kappa \nu$, the Reynolds number $Re \equiv UH/\nu$, the Prandtl number $Pr \equiv \nu/\kappa$ and the aspect ratios of the rectangular container $\Gamma_{xz} \equiv W/H$ and $\Gamma_{yz} \equiv L/H$. Here β denotes the isobaric thermal expansion coefficient, g the acceleration due to gravity, ΔT the applied temperature difference, κ the thermal diffusivity, ν the kinematic viscosity, U the characteristic velocity, W the width, L the length and H the height of the cell. An additional parameter to describe MC is the Archimedes number $Ar = Ra/(Re^2 \times Pr) = \Delta T \beta g H^3 / U^2$, which is the ratio of buoyancy to inertia forces. For $Ar \ll 1$ the flow is primarily driven by inertia forces, for $Ar \gg 1$ the flow is dominated by buoyancy forces. Flows with $Ar \approx 1$ are termed MC.

2. Experimental Setup

To cover a large parameter range of $600 < Re < 3 \times 10^6$ and $1 \times 10^5 < Ra < 1 \times 10^{11}$ two convection cells have been constructed using air as working fluid under different pressure

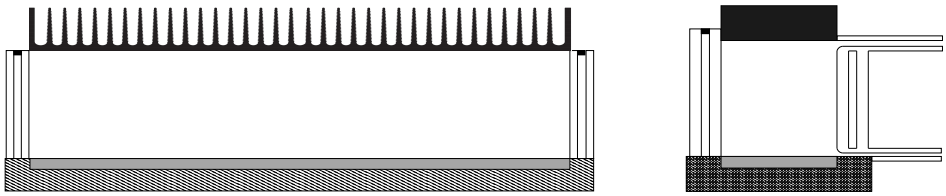

Figure 1: Sketch of the convection cell. Left: Longitudinal cross section. The heating plate is located at the bottom and cooling device at the top. Left: Vertical cross section. The air inlet is placed at the top and the air outlet at the bottom of the cell.

conditions with an aspect ratio of $\Gamma_{\mathrm{xy}} = 1$ and $\Gamma_{\mathrm{xz}} = 5$. The cells are equipped with an air inlet at the top and an air outlet at the bottom. The in- and outlet channels have a rectangular cross section and are located at the same side of the cell. They span the whole length of the cell. The inlet channel has a height of $H_{\mathrm{in}} = \frac{1}{20} \times H$ and a length of $L_{\mathrm{in}} = 30 \times H_{\mathrm{in}}$ to assure a well defined, fully developed channel flow, while the outlet channel has a height of $H_{\mathrm{out}} = \frac{3}{5} \times H_{\mathrm{in}}$ and a length of $L_{\mathrm{out}} = 30 \times H_{\mathrm{out}}$. All side walls are thermally insulated by a layer system with an insulating sheath of air between two transparent windows. Hence we nearly realise adiabatic boundary conditions while maintaining the optical accessibility of the cell. The bottom is equipped with a heating plate and the top with a heat exchanger consisting of an aluminium body with cooling fins. One of the cells with the dimensions $W \times H \times L = 0.1\ \mathrm{m} \times 0.1\ \mathrm{m} \times 0.5\ \mathrm{m}$ was designed to be operated under high pressure conditions of up to 100 bar. The second convection cell has been constructed to work under ambient pressure conditions with the same aspect ratio, but its dimensions are scaled up by a factor of 5.

In this article velocity fields measured by Particle Image Velocimetry (PIV) in the large cell under ambient pressure are presented, analysed and compared to results of temperature measurements conducted in the small cell at 10 bar. Two-dimensional two-component (2D2C) PIV has been carried out in different cross sections. Additionally two-dimensional three-component (2D3C) PIV has been performed in a longitudinal cross section. The 2D2C measurement planes are located at $0.5 \times L$, $0.375 \times L$, $0.25 \times L$ and $0.1 \times L$ while the 2D3C cross section is located at $0.5 \times W$. The instantaneous velocity fields have been acquired with a repetition rate of $2/3$ Hz. For the forced and mix convection case 800 and 4800 instantaneous velocity fields have been evaluated, respectively. Addionally results of a Proper Orthogonal Decomposion (POD) of the instantaneous velocity fields are presented, which have been calculated using the snapshots method by Sirovich [4]. In the following figures the velocity-components are normalised with the buoyancy velocity $V_b = \sqrt{\beta\ H^3\ \Delta T\ g}$ and for sake of visibility only every seventh velocity vector is plotted.

3. Results

One mechanism of heat transport in MC is FC induced by a pressure gradient between in- and outlet. As a result a nearly two-dimensional and particularly in the core region stationary role structure develops. The FC mean wind for $Re = 1.0 \times 10^4$ is shown in figure 2 (left), where a jet of incoming air from the inlet (upper right corner) can be observed. In the following figures the velocity-components are normalised with the buoyancy velocity $V_b = \sqrt{\beta\ H^3\ \Delta T\ g}$ and for sake of visibility only every seventh velocity vector is plotted. As a result a rotating mean wind with a core located near the centre of the cross section develops. The velocity profiles of the v-component at $Y = 0.55 \times H$ in several cross-sections (see fig. 2 right) clearly show the two-dimensional nature of the FC mean wind. For all four cross sections the profiles in FC are

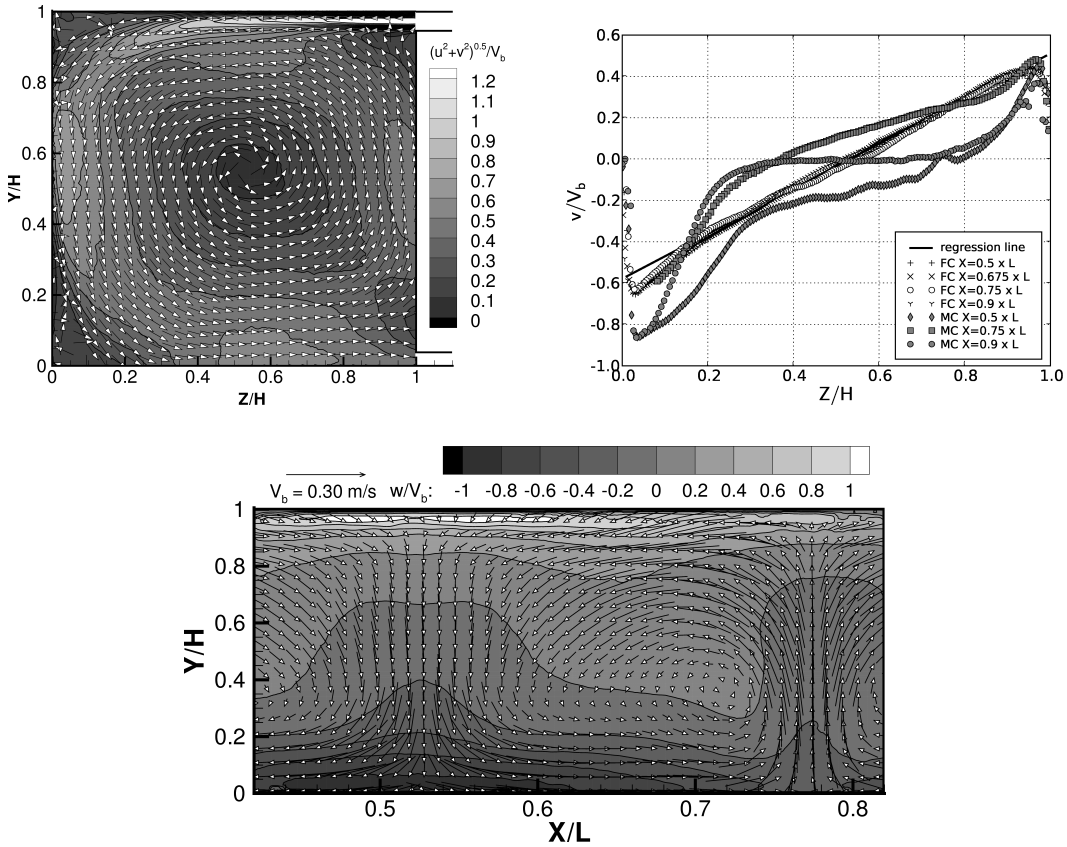

Figure 2: Left: Time averaged velocity field of forced convection at $Ar = 0$ with $Re = 1.0 \times 10^4$ at $0.5 \times L$. Right: Velocity profile of the v-component at FC and MC at $Y = 0.55 \times H$ in several cross sections. Bottom: Time averaged velocity field at MC.

nearly congruent. The profiles also reveal the linear relation between the distance from the LSC centre $(\underline{x} - \underline{x}_0)$ and the velocity v. From this it can be concluded that the mean wind behaves in the core like a solid body (Rankine vortex).

The other mechanism that drives the heat transport in MC is the buoyancy force. Rising hot plumes from the bottom thermal boundary layer and falling cold plumes emitted at the top boundary layer are developed. As a result of this plume-motion a LSC is formed [3]. In the given enclosure falling plumes have been generated at the left $X = 0$ and right $X = L$ side walls as well as at $X = 0.5 \times L$. Rising plumes are located at $X = 0.25 \times L$ and $X = 0.75 \times L$. As a consequence, the plume-motion induces four large-scale circulating role structures, which are arranged in longitudinal direction. One of these LSCs located between $X = 0.4 \times L$ and $X = 0.8 \times L$ is presented in fig. 2 bottom showing the time averaged velocity map of 4800 instantaneous velocity fields (the images have been recorded with a repetition rate of $2/3$ Hz). The contour map in the figure depicts the out-of-plane component of the velocity w.

Comparing the velocity fields obtained for FC with the ones for MC a breakdown of the 2D mean wind and the solid body rotation can be observed (see fig. 2 right). Analysing the measured temperature data spatial temperature variations over the length of the outlet depending on the orientation of the buoyancy induced LSCs have been found. In regions of rising plumes T_{out} is elevated and in regions where plumes are falling a lower T_{out} can be observed. For $Ar > 1$, the temperature signal locally fluctuates in time (subplot Fig. 3). The corresponding power-spectrum of the local temperature fluctuations at $0.5 \times L$ (Fig. 3) reveals two characteristic

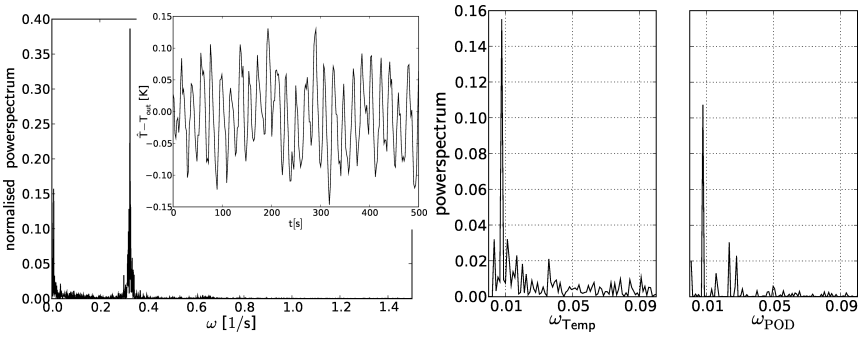

Figure 3: Left: Powerspectrum of T_{out} at $0.5 \times L$ for $Ar = 3.3$, $Ra = 2.4 \times 10^8$ and $Re = 1 \times 10^4$ at 10 bar. The subplot shows the first 500 of 5000 s of the time series of the outlet temperature ($0.5 \times L$). Right: Powerspectrum of the low frequency oscillations of T_{out} and the powerspectrum of $\underline{\zeta}_1^{\mathrm{MC}}$.

frequencies. One of these characteristic frequencies is $\omega = 0.32\ \mathrm{s}^{-1}$, which equals the angular frequency $\omega_{\mathrm{FC}} = 0.32\ \mathrm{s}^{-1}$ of the role structure found in the PIV results of forced convection in the large cell. Although the temperature measurements were performed at 10 bar (small cell experiment), the same frequency appears and we assume this frequency to be associated with the dynamics of the role structure induced by forced convection. The second characteristic frequency $\omega_{\mathrm{low}} = 0.008\ \mathrm{s}^{-1}$ (Fig. 3) is much lower than ω_{FC}, as well as the estimated angular frequency $\omega_{\mathrm{TC}} \approx 0.5\ \mathrm{s}^{-1}$ associated with the thermal convection induced LSCs in fig. 2 (bottom).

To investigate if these frequencies are related to the dynamics of any characteristic flow structures a POD analysis of the 2D3C PIV data obtained for forced and mixed convection has been performed. For both, forced and mixed convection, eigenfunctions with eigenvalues $\lambda_1^{\mathrm{MC}} = 73$ % and $\lambda_1^{\mathrm{FC}} = 90$ % of the total energy were obtained. Additionally the coefficient of the eigenfunction $\underline{\zeta}$ which corresponds to the highest eigenvalue has been analysed. The powerspectrum $\underline{\zeta}_1$ of the forced convection case reveals no characteristic frequency contrarily to the powerspectrum of the mixed convection case. The latter contains the same low characteristic frequency that has been found in the temperature measurements at 10 bar. Due to the concurrence of these frequencies it is concluded that this low frequency oscillation in the heat transfer is the result of the dynamics of the buoyancy induced LSCs. Even more, we assume that the oscillations are a result of torsional oscillations of the buoyancy induced LSCs in agreement with findings in Rayleigh-Bénard convection by Funfschilling et al. [2].

On the conference and in the full length paper the Ar dependency of the LSCs and the low frequency oscillations for $1 < Ar < 3.3$ will be discussed in detail.

References

1. P. F. Linden, The fluid mechanics of natural ventilation, Annu. Rev. Fluid Mech., **31,** 201, 1999.
2. D. Funfschilling, E. Brown and G. Ahlers, Torsional oscillations of the large-scale circulation in turbulent Rayleigh-Bénard convection, J. Fluid Mech., **607,** 119, 2008.
3. X.-L. Qui and P. Tong, Large-scale velocity structures in turbulent thermal convection, Phys. Rev. E, **64,** 036304, 2001.
4. L. Sirovich. Turbulence and the dynamics of coherent structures part ii: Symmetries and transformation, Quarterly of Applied Mathematics, **45(3),** 573, 1987.